ACS APPLIED MATERIALS & INTERFACES

www.acsami.org

Research Article

Visibly Transparent Solar Windows Based on Colloidal Silicon Quantum Dots and Front-Facing Silicon Photovoltaic Cells

Shanshan Han, Guo Chen, Chunhui Shou, Hao Peng, Shengli Jin, and Chang-Ching Tu*

Cite This: *ACS Appl. Mater. Interfaces* 2020, 12, 43771−43777

Read Online

ACCESS | Metrics & More | Article Recommendations | Supporting Information

ABSTRACT: We demonstrate luminescent solar concentrators (LSCs) based on colloidal silicon quantum dots (SiQDs) as UV-selective fluorophores and coupled with front-facing silicon photovoltaic cells for the solar window application. The visibly transparent LSC composed of a thin layer of liquid SiQD suspension sandwiched between two thin glass slabs constitutes the windowpane, while strips of silicon photovoltaic cells with their front surfaces adhering to the LSC rear surface form the window frame. Furthermore, the LSC perimeter is surrounded by reflecting mirrors for preventing the fluorescence from leaking out through the edges. The SiQDs dispersed in 1-octadecene selectively absorb UV light and re-emit red fluorescence with quantum efficiency about 40%. Owing to the negligible overlap between the absorbance and photoluminescence spectra, the reabsorption effect is insignificant. The front-facing silicon photovoltaic strips located at the window frame can produce electricity by harvesting not only solar radiation but also the SiQD-generated fluorescence propagating from the windowpane. For the SiQD-LSC with the total light absorbing area equal to 12 cm × 12 cm and the reflecting mirrors tilted 45°, an overall power conversion efficiency of 2.47% under simulated sunlight can be obtained of which about 6% is contributed by the SiQD fluorescence. Meanwhile, the SiQD-LSC retains high spectral quality with average visible transmission and color rendering index through the windowpane equal to 86% and 94, respectively.

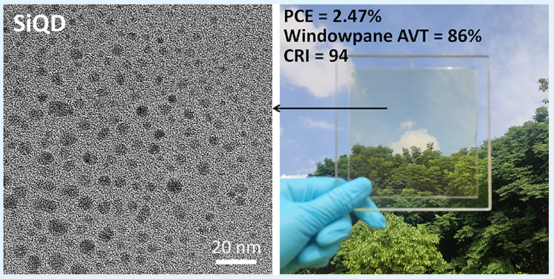

KEYWORDS: *solar windows, luminescent solar concentrators, silicon quantum dots, silicon photovoltaic cells, building-integrated photovoltaics*

INTRODUCTION

Solar windows, which turn ordinary skylights or facades into an extensive network of small electricity generators, play an integral part in the building-integrated photovoltaics (BIPVs), an emerging renewable energy technology to replace or retrofit conventional building components with photovoltaic ones.[1,2] Especially, for those high-rise buildings in the highly urbanized areas, the space for installing ground-based or rooftop solar panels is far from enough to compensate the energy consumption of the buildings themselves. Therefore, to achieve the ultimate goal of "nearly zero energy building",[3] which has been actively pursued by many countries, utilizing the enormous window areas for energy harvesting should be an inevitable approach.

The solar windows, although not as efficient as conventional solar panels, can potentially generate an adequate amount of electricity at the point of use when connected into a large network. At the same time, the solar windows must meet certain safety requirements and maintain translucent, allowing the building occupants to see through and enjoy natural light. Ideally, the solar windows would only absorb and harvest the ultraviolet (UV) and near-infrared (NIR) portions of the solar spectrum, similar to how the low-emissivity coatings on windows alter the incident light spectrum for improving the building energy efficiency.[4]

Several transparent photovoltaic technologies have emerged for the solar window application, some of which have been already commercialized by companies, such as Onyx Solar, Ubiquitous Energy, SolarWindow Technologies, and UbiQD. Among them, the spatially segmented or neutral-colored silicon thin-film technologies have gained the most traction in the solar window market.[5−7] In addition, semitransparent thin films based on organic[8−11] and organic−inorganic hybrid materials[12−15] (such as perovskite-based and dye-sensitized photovoltaic cells) have recently drawn much attention, although their long-term stability has to be improved before the widespread deployment can be realized. These thin film devices, while being capable of achieving high power conversion efficiencies (PCEs) up to 14%,[14] have broad

Received: July 14, 2020
Accepted: September 8, 2020
Published: September 8, 2020

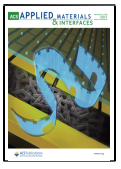

https://dx.doi.org/10.1021/acsami.0c12717
ACS Appl. Mater. Interfaces 2020, 12, 43771−43777

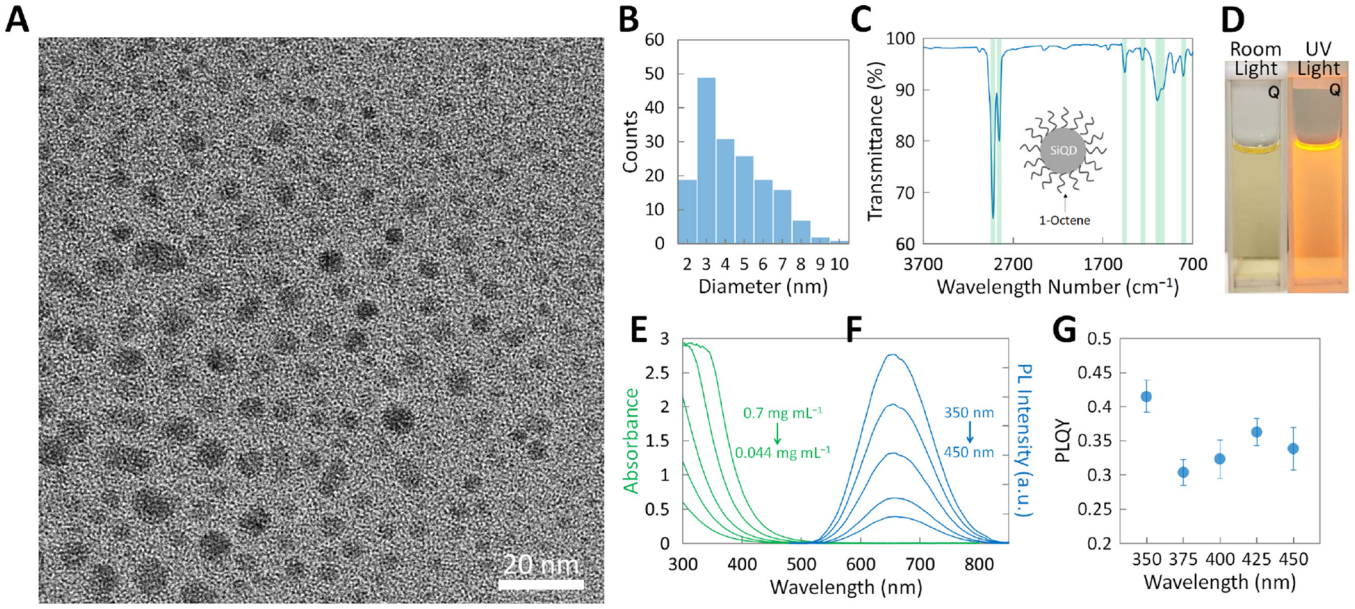

Figure 1. (A) TEM image of the SiQDs. (B) Size distribution of the SiQDs. (C) FTIR spectrum of the SiQDs. The green highlighted areas from left to right correspond to CH_2 asymmetric stretching (2925 cm^{-1}), CH_2 symmetric stretching (2855 cm^{-1}), CH_2 bending (1460 cm^{-1}), Si−C stretching (1255 cm^{-1}), Si−O−Si asymmetric stretching (1090 cm^{-1}), Si−O−C stretching (1040 cm^{-1}), and Si−O−Si symmetric stretching (800 cm^{-1}). Inset: illustration for the SiQD surface chemistry. (D) Photographs of the SiQD suspension in 1-octadecene under room light (left) and 365 nm UV light (right) illumination. (E) Absorbance spectra of the SiQD suspension in 1-octadecene with concentrations about 0.7, 0.35, 0.175, 0.088, and 0.044 mg mL^{-1} (from top to bottom). (F) PL spectra of the SiQD suspension in 1-octadecene with 350, 375, 400, 425, and 450 nm excitation wavelengths (from top to bottom). (G) PLQY versus excitation wavelength for the SiQD suspension in 1-octadecene. The PLQYs were measured using a spectrofluorometer coupled with an integrating sphere. The optical system was precalibrated with rhodamine 6G in ethanol (PLQY = 93.13 ± 2.77%).

absorption of the solar spectrum including the visible range, leading to relatively low average visible transmission (AVT).

On the other hand, visibly transparent luminescent solar concentrators (LSCs)[16−19] with selective absorption in the UV and/or NIR ranges can easily achieve AVT higher than 50%, which is a preferential characteristic for applications where visible transmittance matters, such as windows of buildings and vehicles.[1,2] Furthermore, because of the simple structure, typically a waveguiding plastic or glass slab coated or embedded with fluorophores, the LSCs can seamlessly replace or retrofit existing windows without degrading its original aesthetic quality. Under sunlight, the fluorophores emit fluorescence, which is then guided by the LSC through the total internal reflection toward the edges where the fluorescence is converted into electricity by conventional photovoltaic cells.[20] With the LSC sidewall area where the photovoltaic cells are mounted much smaller than the LSC front surface area, the photon flux received by the photovoltaic cells is concentrated while a much less photovoltaic material is needed.

The LSC performance can be evaluated from two main aspects, conversion efficiency (such as PCE and optical efficiency) and spectral quality (such as AVT and color rendering index, CRI). In general, the two are inversely related to each other.[1] To achieve high conversion efficiency without sacrificing the spectral quality, the fluorophores used in the LSC need to have not only high photoluminescence quantum efficiency (PLQY) but also selective absorption outside the visible range and large Stokes shift for mitigating the reabsorption effect, which is often the major loss mechanism of LSCs. For a single junction, UV- and NIR-selective LSCs with 100% AVT, the thermodynamic limit of the PCE can be as high as 21%.[21] Recently, a wide variety of fluorophores possessing the aforementioned optical properties have been explored to implement efficient and visibly transparent LSCs for the solar window application, including organic dyes,[15,16] phosphorescent nanocrystals,[17] sustainable natural organic molecules,[22] carbon nanodots,[23,24] perovskite quantum dots,[25,26] two-dimensional quantum dots,[27] and other heavy metal-free quantum dots.[18,28−30] Furthermore, some biomimetic ultrathin and flexible solar cells can also be applied for the BIPVs.[31]

In this work, we propose a novel solar window scheme, which combines the concepts of spatially segmented PVs and visibly transparent LSCs. Instead of being positioned in the middle,[32,33] front-facing Si PV strips are placed along the perimeter to form the window frame, while a visibly transparent LSC composed of a thin layer of liquid silicon quantum dot (SiQD) suspension sandwiched between two thin glass slabs constitutes the windowpane. Under sunlight, the front-facing Si PV strips form the window frame function as conventional solar cells. At the same time, the colloidal SiQDs in the windowpane selectively absorb UV light and convert it to red fluorescence with high quantum efficiency. Through the inherent waveguiding structure of the LSC and the reflecting mirrors along the LSC edges, the SiQD-generated fluorescence is directed to the front-facing Si PV strips, thus enhancing the overall PCE. Furthermore, since the SiQDs selectively absorb UV light, the propagating red fluorescence is hardly reabsorbed and the sunlight passing through the windowpane retains exceptionally high AVT and CRI.

https://dx.doi.org/10.1021/acsami.0c12717
ACS Appl. Mater. Interfaces 2020, 12, 43771−43777

EXPERIMENTAL RESULTS

Synthesis and Characterization of the SiQDs. The synthesis of SiQDs was based on an electrochemical etching method developed previously but with some modifications (Supporting Information, Figure S1).[34] First, a p-type crystalline silicon wafer was electrochemically etched in an electrolyte containing hydrofluoric acid and methanol followed by a white light-induced hydrosilylation reaction with neat 1-octene in an oxygen-free environment.[35] Then, the photoluminescent porous silicon layer along with 1-octene was removed from the wafer surface and transferred to a zirconia milling jar for high-energy ball milling. The resulting turbid suspension was centrifuged, and only its translucent supernatant was collected. Finally, the 1-octene solvent was fully evaporated using a rotary evaporator, and the SiQDs were redispersed in 1-octadecene for the following experiments. About 20 mg of the SiQDs can be produced each batch using a 6 in. silicon wafer, and the silicon wafer can be reused until it is electrochemically etched through.

Since the white light-induced hydrosilylation reaction occurs only on the photoluminescent silicon surfaces but not on the nonemissive bulk silicon surfaces,[35] the photoluminescent SiQDs were passivated with 1-octene and therefore able to be retained in the supernatant after centrifugation, whereas all other silicon nanoparticles with relatively hydrophilic oxide capping could not maintain suspension in the nonpolar 1-octene and therefore were precipitated by centrifugation. As shown in the transmission electron microscopy (TEM) image (Figure 1A) and the corresponding size distribution (Figure 1B), in general, the SiQDs have spherical or elliptical shapes with sizes less than 5 nm. Considering that the exciton Bohr radius of silicon is about 5 nm, the nanoparticles with sizes more than 5 nm are either clusters of smaller size silicon quantum dots or nonradiative ones. Based on the fast Fourier transform (FFT) electron diffraction pattern and the interplanar spacing deduced from the high-resolution TEM image (Supporting Information, Figure S2), we may conclude that all nanoparticles here regardless of their sizes are composed of crystalline silicon. Furthermore, the X-ray diffraction (XRD) analysis shows that the SiQD powder is polycrystalline despite the fact that the Si wafer as the starting material is single crystalline (Supporting Information, Figure S3). Such crystallinity transformation has also been observed for the high-energy ball-milled Si nanoparticles.[36] The Fourier transform infrared (FTIR) spectrum (Figure 1C) confirms that the SiQDs are grafted with the 1-octene molecules through hydrosilylation, as evidenced by the strong absorption peaks associated with the CH_2 and Si−C bonds. In addition, the intrinsic surface chemistry of the SiQDs is correlated with the Si−O−Si bridge bonds, which is consistent with all our previous samples also prepared by the electrochemical etching method but without the centrifugation purification step.[34,37]

Due to the small particle size and 1-octene ligand passivation, the SiQDs can form uniform and stable suspension in 1-octadecene and many other nonpolar solvents, such as hexane, toluene, and chloroform. The SiQD suspension appears light yellow in color under room light and emits bright red fluorescence under UV (Figure 1D). Based on the absorbance spectra with different concentrations (Figure 1E), the molar extinction coefficient spectrum of the SiQD suspension is obtained (Supporting Information, Figure S4). Particularly, at 350 nm, the molar extinction coefficient of the SiQD suspension is equal to 2.68×10^5 M^{-1} cm^{-1}, which is close to that of 4 nm diameter CdSe quantum dots at the first excitonic absorption,[38] indicating that the SiQDs have comparable light absorbing ability to other direct band gap quantum dots in the UV range. However, the absorption drops significantly at 500 nm, which mitigates reabsorption. The PL peak wavelength of the SiQD suspension is located at around 650 nm and remains constant regardless of the excitation wavelength (Figure 1F). Furthermore, the PL lifetime of the SiQDs is long, about 32.2 μs (Supporting Information, Figure S5). In contrast, the room-temperature PL lifetime of CdSe quantum dots is usually less than 100 ns.[39] Based on the excitation-independent emission and the long PL lifetime, in addition to the Si−O−Si bridge bonds observed on the SiQD surfaces (Figure 1C), we may conclude that the SiQDs emit PL primarily through radiative recombination among oxide-related surface defect states.[34,40] Lastly, the SiQD suspension in 1-octadecene shows PLQYs about 30 to 40% depending on the excitation wavelengths (Figure 1G). With 350 nm excitation wavelength, the PLQY is about 42%.

Structure and Working Principle of the SiQD-LSCs. The SiQD-LSC is composed of three parts, including a front glass slab, a PMMA ring, and a rear glass slab (Figure 2A). Both the front and rear glass slabs are 1 mm thick, while the PMMA ring is 2 mm thick. The void structure formed by the two glass slabs and the PMMA ring is filled with the SiQD suspension in 1-octadecene. The central square region containing the SiQD suspension (area = $W_{LSC} \times W_{LSC}$) is defined as the windowpane, while the Si PV strips (width = 1 cm) adhering to the SiQD-LSC rear surface form the window frame. Furthermore, the SiQD-LSC perimeter is surrounded by reflecting mirrors for preventing the fluorescence from leaking out through the edges. In this work, the reflecting mirrors are tilted either 45 or 0° (Figure 2B). The fluorescence images viewing from the rear sides of the SiQD-LSCs (W_{LSC} = 10 cm) show the qualitative difference between the two configurations (Figure 2C and Supporting Information, Figure S6). When the reflecting mirrors are tilted 45°, the red fluorescence is reflected out to where the Si PV is located. In contrast, when the reflecting mirrors are perpendicular to the LSC, the red fluorescence propagating to the edges is reflected back into the waveguide. Therefore, more fluorescence escaping from the windowpane was observed.

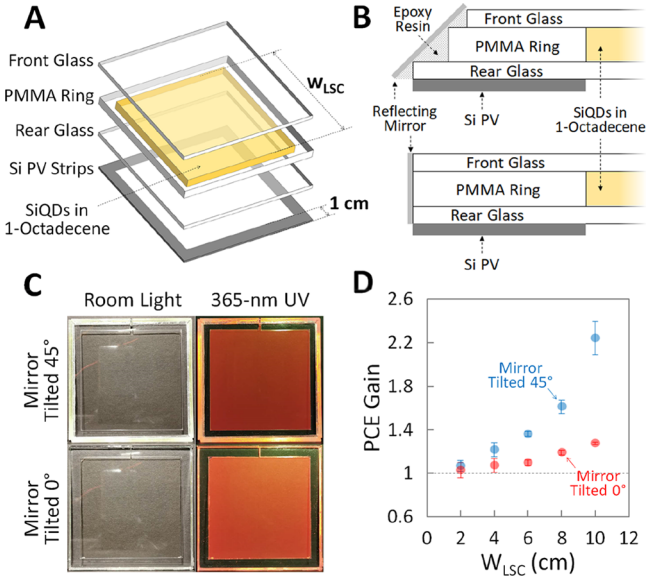

Figure 2. (A) Expanded 3D view of the SiQD-LSC (reflecting mirrors not shown), consisting of a front glass slab (1 mm thick), a PMMA ring (2 mm thick), and a rear glass slab (1 mm thick). The void structure formed by the two glass slabs and the PMMA ring is filled with the SiQD suspension. The central square region containing the SiQD suspension (area = $W_{LSC} \times W_{LSC}$) is defined as the windowpane, while the Si PV strips (width = 1 cm) adhering to the SiQD-LSC rear surface form the window frame. (B) Cross-sectional views of the SiQD-LSC edges with the reflecting mirrors tilted 45° (up) and 0° (bottom). (C) Photographs viewing from the rear sides of the SiQD-LSCs. Under 365 nm UV illumination, the SiQD-LSC with the reflecting mirrors tilted 45° shows more red fluorescence reflected out along the window frame, while the SiQD-LSC with the reflecting mirrors tilted 0° shows more red fluorescence escaping from the windowpane. (D) PCE gains of different-size SiQD-LSCs with the reflecting mirrors tilted 45° (blue circles) and 0° (red circles) under the 365 nm UV illumination with an intensity equal to 0.97 mW cm^{-2}. Here, the concentration of the SiQD suspension is about 0.7 mg mL^{-1}.

https://dx.doi.org/10.1021/acsami.0c12717
ACS Appl. Mater. Interfaces 2020, 12, 43771−43777

Under illumination, the front-facing Si PV can generate electricity by harvesting the light incident on the window frame. At the same time, the fluorescence generated by the SiQDs inside the windowpane can also propagate to the Si PV and enhance its efficiency. The enhancement can be quantified by PCE gain, which is defined as the PCE of the Si PV measured with the SiQD suspension loaded in the windowpane divided by that measured with pure 1-octadecene loaded in the windowpane. To avoid the complication of wiring, for each LSC, we placed only one Si PV strip, mechanically diced from a conventional monocrystalline silicon solar cell wafer, along one LSC edge (Supporting Information, Figure S7). The bare Si PV strip has PCE = 13.27 ± 0.55% under the simulated sunlight in this work. The overall PCE is calculated with the total light absorbing area equal to $(W_{LSC} + 2\ cm) \times (W_{LSC} + 2\ cm)$ and the total electricity generated equal to that generated by one Si PV strip multiplied by four. A similar analysis approach has been adopted in literature.[28]

PCE Gain and Optical Efficiency of the SiQD-LSCs. To understand how the windowpane size affects the enhancement, we studied the PCE gain at different W_{LSC} values under 365 nm UV illumination (Figure 2D and Supporting Information, Table S1). For each W_{LSC} size, the same LSC filled with either the SiQD suspension or pure 1-octadecene was used for measuring the PCE gain. In general, a larger light absorbing area leads to more fluorescence generated inside the windowpane and thus the higher enhancement of the Si PV. Particularly, at W_{LSC} = 10 cm, the PCE gains can be as high as 2.24 and 1.28 with the reflecting mirrors tilted 45 and 0°, respectively. However, as the W_{LSC} drops below 2 cm, the PCE gains approach to unity. Furthermore, the optical efficiency (η_{opt}), here defined as the percentage of the fluorescence photons inside the windowpane able to propagate to and be received by the Si PV, can be calculated using the equation as follows: $4 \times \Delta I_{SC}/q = I_{light} \times W_{LSC}^2 \times A_{SiQD}/h\nu_{365nm} \times \varnothing_{PL} \times \eta_{opt} \times \varnothing_{PV}$, where ΔI_{SC} represents the short-circuit current difference of one Si PV strip measured with and without SiQDs (Supporting Information, Table S1), q is the electron charge (1.6×10^{-19} C), I_{light} is the 365 nm incident light intensity (0.97 mW cm^{-2}), A_{SiQD} is the absorption of the SiQDs at 365 nm (50%; Supporting Information, Figure S8A), $h\nu_{365nm}$ is the 365 nm photon energy (5.44×10^{-19} J), $\varnothing_{PL}$ is the PLQY of the SiQD suspension at 365 nm (about 0.35, Figure 1G), and $\varnothing_{PV}$ is the quantum efficiency of the Si PV at 650 nm (about 0.95).

For the SiQD-LSC with W_{LSC} = 10 cm and the reflecting mirrors tilted 45°, the η_{opt} is estimated to be 49%, whereas the maximum theoretical value of the η_{opt} defined by Snell's law is 72% (Supporting Information, Figure S9). In other words, excluding the 28% escape cone loss, about 32% of the propagating fluorescence photons are lost as they propagate through the waveguide by the total internal reflection and eventually get absorbed by the Si PV. The mechanisms for losing the propagating fluorescence photons might include: (1) reabsorption of the SiQDs, (2) absorption of the glass slabs, (3) scattering due to imperfect waveguide structures, and (4) nonideal reflection at the reflecting mirrors (Supporting Information, Figure S6C). For comparison, for the SiQD-LSC with the same W_{LSC} size (10 cm) but with the reflecting mirrors tilted 0°, the η_{opt} is estimated to be 28%, which is much lower than the η_{opt} (49%) obtained with the reflecting mirrors tilted 45°. As the fluorescence photons propagating toward the edges are reflected back into the waveguide, the chance of optical loss due to the aforementioned mechanisms becomes higher. The stronger red fluorescence escaping from the windowpane, as shown in Figure 2C, is one manifestation.

Optical Loss Analysis for the SiQD-LSCs. To further analyze the optical loss, we characterized the PL emitted from the SiQD-LSC edge when only a slit of the windowpane was exposed to the 365 nm UV illumination (Figure 3 and Supporting Information, Figure S10). The PL spectra were obtained using a multimode quartz optical fiber (numerical aperture = 0.22) with one end affixed to the SiQD-LSC edge and the other end coupled to a spectrofluorometer, which is composed of a monochromator and a photomultiplier tube (PMT). The relative position between the fiber and the SiQD-LSC edge was kept constant at all times, and the small gap between the two parts was filled with immersion lens oil (refractive index = 1.52) to facilitate

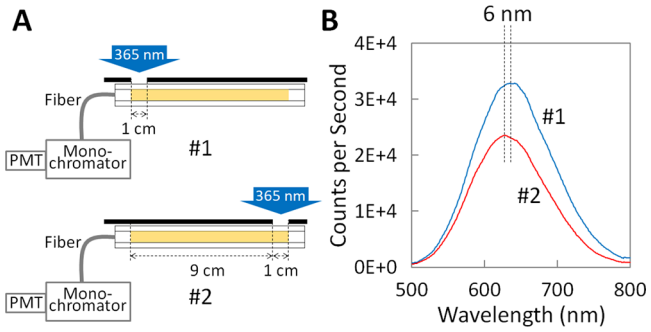

Figure 3. (A) Schematic showing the two different slit configurations and the optical setup for measuring the PL spectra at the SiQD-LSC edge. (B) PL spectra measured with the two slit configurations. The PL spectrum measured with the slit configuration #2 (red curve) exhibits 6 nm blueshift of the PL peak and about a 30% smaller integrated area compared to that measured with the slit configuration #1 (blue curve). Here, the 365 nm UV light intensities incident on the two slit areas are both equal to 4 mW cm^{-2} and the SiQD concentration is about 0.7 mg mL^{-1}.

the fluorescence entering the fiber. With the slit 9 cm away from the window frame (#2 in Figure 3), the PL spectrum exhibits 6 nm blueshift of the PL peak compared to that obtained with the slit right next to the window frame (#1 in Figure 3). The observed blueshift should result from the absorption of the soda–lime glass slabs, which show stronger absorption in the red spectral range (Supporting Information, Figure S8C). Although both the front and rear glass slabs are thin (1 mm), considering the fact that numerous total internal reflections might be necessary for a red fluorescence light beam to reach the LSC edge, the accumulated glass thickness the light beam travels through can be large. Unlike most other LSCs, here, the SiQD reabsorption is less prominent relative to the glass absorption because based on the absorbance spectrum in Figure 1E, the SiQD reabsorption should lead to PL redshift instead of blueshift as observed in Figure 3B. Furthermore, due to the negligible overlap between the absorbance and PL spectra of the SiQD suspension (Figure 1E,F) and the small molar extinction coefficients at wavelengths longer than 500 nm (Supporting Information, Figure S4), the reabsorption effect in this work should be insignificant. Lastly, the PL spectrum measured with the slit configuration #2 has about a 30% smaller integrated area than that measured with the slit configuration #1, indicating that about 30% of the fluorescence photons are lost as they propagate over a distance of 9 cm in the windowpane. In practice, the average propagating distance of the fluorescence photons in a 10 cm × 10 cm windowpane should be less than 9 cm. However, taking into consideration of other potential loss at the LSC edges, the windowpane loss analysis here is consistent with the previously estimated optical efficiency (η_{opt} = 49%; i.e., about 32% of the propagating fluorescence photons are lost before being received by the Si PV) for the SiQD-LSC with W_{LSC} = 10 cm and the reflecting mirrors tilted 45°.

Wavelength-Resolved Analysis for the SiQD-LSCs. Next, we characterized the PCE gains and the overall PCEs of the SiQD-LSCs (W_{LSC} = 10 cm) under 365, 465, 525, and 625 nm single-wavelength illumination (Figure 4 and Supporting Information, Table S2). In general, the SiQD-LSC with the reflecting mirrors tilted 45°, compared to tilted 0°, shows higher PCE gains due to the higher optical efficiency (η_{opt} = 49% versus 28%) but relatively lower overall PCEs because the Si PV strip is partially shadowed by the tilted mirror (Figure 2B). Furthermore, the PCE gain is highly correlated to the SiQD absorption (green curves in Figure 4A,B and Supporting Information, Figure S8A), confirming that the gain results from the SiQD fluorescence. On the other hand, the overall PCEs of the SiQD-LSCs without SiQDs in the windowpane (green and orange curves in Figure 4C,D, respectively) are mainly determined by the transmission through the window frame region (Supporting Information, Figure

https://dx.doi.org/10.1021/acsami.0c12717
ACS Appl. Mater. Interfaces 2020, 12, 43771–43777

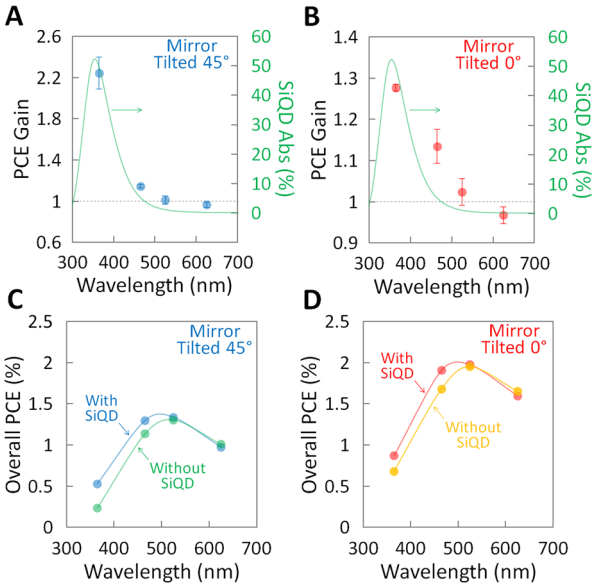

Figure 4. (A, B) PCE gain versus illumination wavelengths (365, 465, 525, and 625 nm) for the SiQD-LSCs (W_{LSC} = 10 cm) with the reflecting mirrors tilted 45 and 0°, respectively. Here, the single-wavelength light sources are 365, 465, 525, and 625 nm high-power light-emitting diodes with the light intensities incident on the SiQD-LSC surface equal to 0.97, 0.93, 1.00, and 0.84 mW cm^{-2}, respectively. The SiQD concentration is about 0.7 mg mL^{-1}. The green curves represent the absorption of the SiQDs in the windowpane, as calculated in the Supporting Information (Figure S8A). (C, D) Overall PCE versus illumination wavelengths (365, 465, 525, and 625 nm) for the SiQD-LSCs (W_{LSC} = 10 cm) with the reflecting mirrors tilted 45 and 0°, respectively. The blue and red curves represent the overall PCEs measured with SiQDs, while the green and orange curves represent the overall PCEs measured without SiQDs.

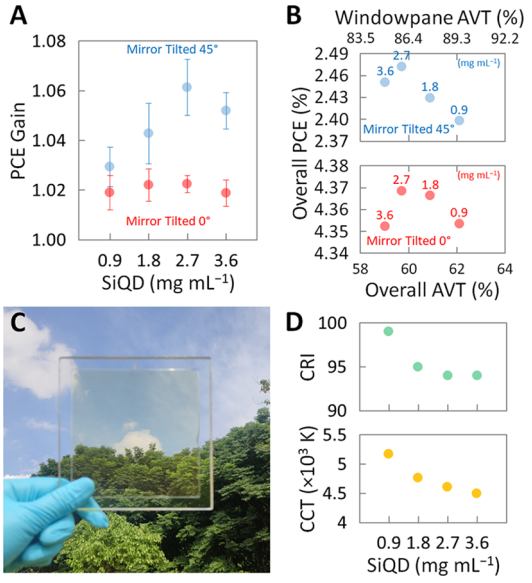

Figure 5. (A) PCE gain versus SiQD concentrations (0.9, 1.8, 2.7, and 3.6 mg mL^{-1}) for the SiQD-LSCs (W_{LSC} = 10 cm) under simulated sunlight. The blue and red circles represent the reflecting mirrors tilted 45 and 0°, respectively. Here, the simulated sunlight is produced by a conventional xenon lamp with the light intensity incident on the SiQD-LSC surface equal to 6.51 mW cm^{-2}. (B) Overall PCE versus windowpane AVT or overall AVT (windowpane AVT × $10^2/12^2$) for the same SiQD-LSCs in (A). For each data point, the corresponding SiQD concentration is labeled. (C) Photograph showing a scenic view seen through the windowpane of the SiQD-LSC (W_{LSC} = 10 cm and SiQD concentration = 2.7 mg mL^{-1}). (D) CRI and CCT of the SiQD-LSCs with different SiQD concentrations. The spectra used for calculating the AVT, CRI, and CCT values are shown in the Supporting Information (Figure S11).

S8B), which increases from the UV to green spectral range and then slightly declines in the red spectral range due to the glass slab absorption. Under 365 and 465 nm illumination where the PCE gains are obvious, the overall PCEs measured with SiQDs in the windowpane (blue and red curves in Figure 4C,D, respectively) are higher than those measured without SiQDs. Under 525 nm illumination, the PCE gains approach unity, whereas the overall PCEs reach their maxima equal to 1.3 and 2% for the SiQD-LSCs with the reflecting mirrors tilted 45 and 0°, respectively.

SiQD-LSC Performance under Simulated Sunlight. In addition to the wavelength-resolved analysis, we characterized the PCE gains and the overall PCEs of the SiQD-LSCs (W_{LSC} = 10 cm) under simulated sunlight, while the concentration of the SiQD suspension varies (Figure 5A,B and Supporting Information, Table S3). Similar to the previous single-wavelength experiment, the SiQD-LSC with the reflecting mirrors tilted 45°, compared to tilted 0°, shows higher PCE gains but relatively lower overall PCEs. Furthermore, the PCE gain and the overall PCE increase as the SiQD concentration increases because of more fluorescence generated inside the windowpane. However, when the SiQD concentration is too high, the SiQD absorption particularly in the UV range saturates (Supporting Information, Figure S11A); that is, a further increase in the SiQD concentration does not lead to more fluorescence generated. On the other hand, owing to the high SiQD concentration, the reabsorption effect becomes more serious. As a result, the PCE gain and the overall PCE at 3.6 mg mL^{-1} become lower than at 2.7 mg mL^{-1} for both SiQD-LSCs with the reflecting mirrors tilted 45 and 0°. In terms of spectral properties, since the primary absorption of the SiQD suspension lies in the UV range with little absorption in the visible range (Figure 1E), the AVT and CRI measured at the windowpane region are more than 80 and 90%, respectively, and the correlated color temperature (CCT) is generally above 4000 K (Figure 5B,D and Supporting Information, Figure S11). A scenic view seen through the windowpane is almost identical to that perceived with bare eyes, except for a warmer color tone due to the lower CCT (Figure 5C). In addition, because the window frame consisting of the Si PV strips (width = 1 cm) is totally opaque, the overall AVT can be calculated by multiplying the windowpane AVT with a factor of $10^2/12^2$.

In summary, when the SiQD concentration is equal to 2.7 mg mL^{-1} at which the module is most efficient, the SiQD-LSCs with the reflecting mirrors tilted 45 and 0° show the overall PCEs = 2.47 and 4.37% and PCE gains = 1.06 and 1.02, respectively, while the overall AVT = 60%, CRI = 94, and CCT = 4612 K. Compared to other semitransparent PV solar window technologies, such as the bulk heterojunction organic PVs (PCE = 4%, AVT = 64.4%, and CRI = 94.5) and the NIR-selective excitonic semiconductor PVs (PCE = 5.1%, AVT = 51.5%, and CRI = 65.3),[1,41] the SiQD-LSCs in this work attain similar PCEs while achieving outstanding spectral quality due to the UV-selective absorption of the SiQDs. To compare with other visibly transparent LSCs, a Si PV strip is attached perpendicularly to the edge of the SiQD-LSC (W_{LSC} = 10 cm, SiQD concentration = 2.7 mg mL^{-1}, no reflecting mirror, and no front-facing Si PV) (Supporting Information, Figure S12). Following the same measurement condition as described previously, an overall PCE = 0.13% was obtained and the SiQD-LSC windowpane AVT was equal to 86%. The result is comparable to the NIR-selective organic salt LSCs (PCE = 0.4%, AVT = 88.3%, and CRI = 94.3).[17] By using larger W_{LSC} while keeping the width of the Si PV strips the same, the PCE gain, which is proportional to W_{LSC} as shown in Figure 2D, can be further improved, and the overall AVT becomes closer to the windowpane AVT, as the factor $W_{LSC}^2/(W_{LSC}+2)^2$ getting closer to unity. In addition, if the PV strips have relatively high quantum efficiency in the red spectral

https://dx.doi.org/10.1021/acsami.0c12717
ACS Appl. Mater. Interfaces 2020, 12, 43771−43777

range, which matches well with the SiQD PL spectrum, the PCE gain can be further increased.

CONCLUSIONS

In summary, we demonstrate a novel solar window structure, which combines spatially segmented PVs and visibly transparent LSCs. The windowpane is composed of a thin layer of SiQD suspension sandwiched between two thin glass slabs, while front-facing Si PV strips placed along the LSC perimeter form the window frame. Under sunlight, the front-facing Si PV strips harvest not only solar radiation but also the SiQD-generated fluorescence propagating from the windowpane. The SiQDs (<10 nm) are grafted with 1-octene through hydrosilylation to form uniform and stable suspension in 1-octadecene. The SiQD suspension selectively absorbs UV light with a high molar extinction coefficient equal to 2.68×10^5 M^{-1} cm^{-1} at 350 nm and re-emits red fluorescence (peak at about 650 nm) with the PLQY equal to 42%. In general, the PCE gain of the SiQD-LSC is proportional to the windowpane size (W_{LSC}) and highly correlated to the SiQD absorption. Under 365 nm UV illumination, the PCE gain of the SiQD-LSC (W_{LSC} = 10 cm, SiQD concentration = 0.7 mg mL^{-1}, and reflecting mirrors tilted 45°) can be as high as 2.24, corresponding to the optical efficiencies (η_{opt}) equal to 49%. In comparison, the maximum theoretical η_{opt} defined by Snell's law is 72%. Here, the major optical loss is due to the absorption of the soda−lime glass slabs instead of the SiQD reabsorption. Lastly, under simulated sunlight, the visibly transparent SiQD-LSC (W_{LSC} = 10 cm, SiQD concentration = 2.7 mg mL^{-1}, and reflecting mirrors tilted 45°) exhibits overall PCE = 2.47%, PCE gain = 1.06, windowpane AVT = 86%, overall AVT = 60%, CRI = 94, and CCT = 4612 K. Compared to other solar window technologies, the SiQD-LSCs in this work attain similar PCEs while achieving exceptional spectral quality due to the UV-selective absorption of the SiQDs.

ASSOCIATED CONTENT

Supporting Information

The Supporting Information is available free of charge at https://pubs.acs.org/doi/10.1021/acsami.0c12717.

Synthesis process, high-resolution TEM image, and XRD pattern of the 1-octene-passivated SiQDs; molar extinction coefficient spectrum and PL lifetime of the SiQD suspension in 1-octadecene; schematic and photographs of different-size SiQD-LSCs coupled with Si PV strips; transmission spectra through the windowpane and window frame regions of the SiQD-LSC; escape cone loss analysis; photographs of the SiQD-LSC during optical loss analysis; spectra for calculating AVT, CRI, and CCT; and values of short-circuit current, open-circuit voltage, fill factor, and PCE of the SiQD-LSCs under different conditions of measurement (PDF)

AUTHOR INFORMATION

Corresponding Author

Chang-Ching Tu − *University of Michigan-Shanghai Jiao Tong University Joint Institute, Shanghai Jiao Tong University, Shanghai 200240, China*; Phone: +86-21-34206765; Email: changching.tu@sjtu.edu.cn

Authors

Shanshan Han − *University of Michigan-Shanghai Jiao Tong University Joint Institute, Shanghai Jiao Tong University, Shanghai 200240, China*

Guo Chen − *University of Michigan-Shanghai Jiao Tong University Joint Institute, Shanghai Jiao Tong University, Shanghai 200240, China*

Chunhui Shou − *Zhejiang Energy Group R&D Institute Co., Ltd. and Key Laboratory of Solar Energy Utilization & Energy Saving Technology of Zhejiang Province, Hangzhou, Zhejiang 311121, China*

Hao Peng − *Zhejiang Energy Group R&D Institute Co., Ltd. and Key Laboratory of Solar Energy Utilization & Energy Saving Technology of Zhejiang Province, Hangzhou, Zhejiang 311121, China*

Shengli Jin − *Zhejiang Energy Group R&D Institute Co., Ltd. and Key Laboratory of Solar Energy Utilization & Energy Saving Technology of Zhejiang Province, Hangzhou, Zhejiang 311121, China*

Complete contact information is available at: https://pubs.acs.org/10.1021/acsami.0c12717

Notes

The authors declare no competing financial interest.

ACKNOWLEDGMENTS

This research was financially supported by the Zhejiang Energy Group R&D Institute Co., Ltd. (JSYJY-JS-2019-014).

REFERENCES

(1) Traverse, C. J.; Pandey, R.; Barr, M. C.; Lunt, R. R. Emergence of Highly Transparent Photovoltaics for Distributed Applications. *Nat. Energy* **2017**, *2*, 849−860.

(2) Husain, A. A. F.; Hasan, W. Z. W.; Shafie, S.; Hamidon, M. N.; Pandey, S. S. A Review of Transparent Solar Photovoltaic Technologies. *Renewable Sustainable Energy Rev.* **2018**, *94*, 779−791.

(3) The European Parliament and the Council of the European Union. *Directive 2010/31/EU of the European Parliament and the Council on the energy performance of buildings (recast). Official Journal of the European Union 23*, http://data.europa.eu/eli/dir/2010/31/oj (2010)

(4) Schaefer, C.; Bräuer, G.; Szczyrbowski, J. Low Emissivity Coatings on Architectural Glass. *Surf. Coat. Technol.* **1997**, *93*, 37−45.

(5) Yoon, J.; Baca, A. J.; Park, S.-I.; Elvikis, P.; Geddes, J. B., III; Li, L.; Kim, R. H.; Xiao, J.; Wang, S.; Kim, T.-H.; Motala, M. J.; Ahn, B. Y.; Duoss, E. B.; Lewis, J. A.; Nuzzo, R. G.; Ferreira, P. M.; Huang, Y.; Rockett, A.; Rogers, J. A. Ultrathin Silicon Solar Microcells for Semitransparent, Mechanically Flexible and Microconcentrator Module Designs. *Nat. Mater.* **2008**, *7*, 907−915.

(6) Lim, J. W.; Lee, D. J.; Yun, S. J. Semi-Transparent Amorphous Silicon Solar Cells Using a Thin P-Si Layer and a Buffer Layer. *ECS Solid State Lett.* **2013**, *2*, Q47−Q49.

(7) Lee, K.; Kim, N.; Kim, K.; Um, H.-D.; Jin, W.; Choi, D.; Park, J.; Park, K. J.; Lee, S.; Seo, K. Neutral-Colored Transparent Crystalline Silicon Photovoltaics. *Joule* **2020**, *4*, 235−246.

(8) Zhang, J.; Xu, G.; Tao, F.; Zeng, G.; Zhang, M.; Yang, Y. M.; Li, Y.; Li, Y. Highly Efficient Semitransparent Organic Solar Cells with Color Rendering Index Approaching 100. *Adv. Mater.* **2019**, *31*, 1807159.

(9) Brus, V. V.; Lee, J.; Luginbuhl, B. R.; Ko, S.-J.; Bazan, G. C.; Nguyen, T.-Q. Solution-Processed Semitransparent Organic Photovoltaics: From Molecular Design to Device Performance. *Adv. Mater.* **2019**, *31*, 1900904.

(10) Liu, Y.; Cheng, P.; Li, T.; Wang, R.; Li, Y.; Chang, S.-Y.; Zhu, Y.; Cheng, H.-W.; Wei, K.-H.; Zhan, X.; Sun, B.; Yang, Y. Unraveling

Sunlight by Transparent Organic Semiconductors toward Photovoltaic and Photosynthesis. *ACS Nano* **2019**, *13*, 1071−1077.
(11) Lunt, R. R.; Bulovic, V. Transparent, Near-Infrared Organic Photovoltaic Solar Cells for Window and Energy-Scavenging Applications. *Appl. Phys. Lett.* **2011**, *98*, 113305.
(12) Zuo, L.; Shi, X.; Fu, W.; Jen, A. K.-Y. Highly Efficient Semitransparent Solar Cells with Selective Absorption and Tandem Architecture. *Adv. Mater.* **2019**, *31*, 1901683.
(13) Xue, Q.; Xia, R.; Brabec, C. J.; Yip, H.-L. Recent Advances in Semi-Transparent Polymer and Perovskite Solar Cells for Power Generating Window Applications. *Energy Environ. Sci.* **2018**, *11*, 1688−1709.
(14) Della Gaspera, E.; Peng, Y.; Hou, Q.; Spiccia, L.; Bach, U.; Jasieniak, J. J.; Cheng, Y.-B. Ultra-Thin High Efficiency Semitransparent Perovskite Solar Cells. *Nano Energy* **2015**, *13*, 249−257.
(15) Roy, A.; Ghosh, A.; Bhandari, S.; Selvaraj, P.; Sundaram, S.; Mallick, T. K. Color Comfort Evaluation of Dye-Sensitized Solar Cell (DSSC) Based Building-Integrated Photovoltaic (BIPV) Glazing after 2 Years of Ambient Exposure. *J. Phys. Chem. C* **2019**, *123*, 23834−23837.
(16) Rondão, R.; Frias, A. R.; Correia, S. F. H.; Fu, L.; de Zea Bermudez, V.; André, P. S.; Ferreira, R. A. S.; Carlos, L. D. High-Performance Near-Infrared Luminescent Solar Concentrators. *ACS Appl. Mater. Interfaces* **2017**, *9*, 12540−12546.
(17) Zhao, Y.; Meek, G. A.; Levine, B. G.; Lunt, R. R. Near-Infrared Harvesting Transparent Luminescent Solar Concentrators. *Adv. Opt. Mater.* **2014**, *2*, 606−611.
(18) Zhao, Y.; Lunt, R. R. Transparent Luminescent Solar Concentrators for Large-Area Solar Windows Enabled by Massive Stokes-Shift Nanocluster Phosphors. *Adv. Energy Mater.* **2013**, *3*, 1143−1148.
(19) Erickson, C. S.; Bradshaw, L. R.; McDowall, S.; Gilbertson, J. D.; Gamelin, D. R.; Patrick, D. L. Zero-Reabsorption Doped-Nanocrystal Luminescent Solar Concentrators. *ACS Nano* **2014**, *8*, 3461−3467.
(20) Rafiee, M.; Chandra, S.; Ahmed, H.; McCormack, S. J. An Overview of Various Configurations of Luminescent Solar Concentrators for Photovoltaic Applications. *Opt. Mater.* **2019**, *91*, 212−227.
(21) Yang, C.; Lunt, R. R. Limits of Visibly Transparent Luminescent Solar Concentrators. *Adv. Opt. Mater.* **2017**, *5*, 1600851.
(22) Frias, A. R.; Correia, S. F. H.; Martins, M.; Ventura, S. P. M.; Pecoraro, E.; Ribeiro, S. J. L.; André, P. S.; Ferreira, R. A. S.; Coutinho, J. A. P.; Carlos, L. D. Sustainable Liquid Luminescent Solar Concentrators. *Adv. Sustainable Syst.* **2019**, *3*, 1800134.
(23) Talite, M. J.; Huang, H.-Y.; Cai, K.-B.; Co, K. C. C.; Santoso, P. A. C.; Chang, S.-H.; Chou, W.-C.; Yuan, C.-T. Visible-Transparent Luminescent Solar Concentrators Based on Carbon Nanodots in the Siloxane Matrix with Ultrahigh Quantum Yields and Optical Transparency at High-Loading Contents. *J. Phys. Chem. Lett.* **2020**, *11*, 567−573.
(24) Gong, X.; Ma, W.; Li, Y.; Zhong, L.; Li, W.; Zhao, X. Fabrication of High-Performance Luminescent Solar Concentrators Using N-Doped Carbon Dots/PMMA Mixed Matrix Slab. *Org. Electron.* **2018**, *63*, 237−243.
(25) Zhao, H.; Benetti, D.; Tong, X.; Zhang, H.; Zhou, Y.; Liu, G.; Ma, D.; Sun, S.; Wang, Z. M.; Wang, Y.; Rosei, F. Efficient and Stable Tandem Luminescent Solar Concentrators Based on Carbon Dots and Perovskite Quantum Dots. *Nano Energy* **2018**, *50*, 756−765.
(26) Li, T.-Y.; Xu, X.; Lin, C.-H.; Guan, X.; Hsu, W.-H.; Tsai, M.-L.; Fang, X.; Wu, T.; He, J.-H. Highly UV Resistant Inch-Scale Hybrid Perovskite Quantum Dot Papers. *Sci. Adv.* **2020**, 1902439.
(27) Manikandan, A.; Chen, Y.-Z.; Shen, C.-C.; Sher, C.-W.; Kuo, H.-C.; Chueh, Y.-L. A Critical Review on Two-Dimensional Quantum Dots (2D QDs): From Synthesis toward Applications in Energy and Optoelectronics. *Prog. Quantum Electron.* **2019**, *68*, 100226.
(28) Meinardi, F.; McDaniel, H.; Carulli, F.; Colombo, A.; Velizhanin, K. A.; Makarov, N. S.; Simonutti, R.; Klimov, V. I.; Brovelli, S. Highly Efficient Large-Area Colourless Luminescent Solar Concentrators Using Heavy-Metal-Free Colloidal Quantum Dots. *Nat. Nanotechnol.* **2015**, *10*, 878−885.
(29) Meinardi, F.; Ehrenberg, S.; Dhamo, L.; Carulli, F.; Mauri, M.; Bruni, F.; Simonutti, R.; Kortshagen, U.; Brovelli, S. Highly Efficient Luminescent Solar Concentrators Based on Earth-Abundant Indirect-Bandgap Silicon Quantum Dots. *Nat. Photonics* **2017**, *11*, 177−185.
(30) You, Y.; Tong, X.; Wang, W.; Sun, J.; Yu, P.; Ji, H.; Niu, X.; Wang, Z. M. Eco-Friendly Colloidal Quantum Dot-Based Luminescent Solar Concentrators. *Adv. Sci.* **2019**, *6*, 1801967.
(31) Das, S.; Hossain, M. J.; Leung, S.-F.; Lenox, A.; Jung, Y.; Davis, K.; He, J.-H.; Roy, T. A Leaf-Inspired Photon Management Scheme Using Optically Tuned Bilayer Nanoparticles for Ultra-Thin and Highly Efficient Photovoltaic Devices. *Nano Energy* **2019**, *58*, 47−56.
(32) Bronstein, N. D.; Li, L.; Xu, L.; Yao, Y.; Ferry, V. E.; Alivisatos, A. P.; Nuzzo, R. G. Luminescent Solar Concentration with Semiconductor Nanorods and Transfer-Printed Micro-Silicon Solar Cells. *ACS Nano* **2014**, *8*, 44−53.
(33) Leow, S. W.; Corrado, C.; Osborn, M.; Isaacson, M.; Alers, G.; Carter, S. A. Analyzing Luminescent Solar Concentrators with Front-Facing Photovoltaic Cells Using Weighted Monte Carlo Ray Tracing. *J. Appl. Phys.* **2013**, *113*, 214510.
(34) Tu, C.-C.; Chen, K.-P.; Yang, T.-A.; Chou, M.-Y.; Lin, L. Y.; Li, Y.-K. Silicon Quantum Dot Nanoparticles with Antifouling Coatings for Immunostaining on Live Cancer Cells. *ACS Appl. Mater. Interfaces* **2016**, *8*, 13714−13723.
(35) Stewart, M. P.; Buriak, J. M. Exciton-Mediated Hydrosilylation on Photoluminescent Nanocrystalline Silicon. *J. Am. Chem. Soc.* **2001**, *123*, 7821−7830.
(36) Ye, Z.; Srivastava, P. K.; Xu, Y.; Wang, W.; Jing, L.; Chen, S.-L.; Tu, C.-C. Surface-Functionalized Silicon Nanoparticles as Contrast Agents for Photoacoustic Microscopy Imaging. *ACS Appl. Nano Mater.* **2019**, *2*, 7577−7584.
(37) Srivastava, P. K.; Han, S.; Tu, C.-C.; Jing, L. Phototoxicity Generated by Silicon Quantum Dot Nanoparticles on Zebrafish Embryos. *ACS Appl. Bio Mater.* **2019**, *2*, 2872−2878.
(38) Yu, W. W.; Qu, L.; Guo, W.; Peng, X. Experimental Determination of the Extinction Coefficient of CdTe, CdSe, and CdS Nanocrystals. *Chem. Mater.* **2003**, *15*, 2854−2860.
(39) de Mello Donegá, C.; Bode, M.; Meijerink, A. Size- and Temperature-Dependence of Exciton Lifetimes in CdSe Quantum Dots. *Phys. Rev. B* **2006**, *74*, No. 085320.
(40) Kůsová, K.; Cibulka, O.; Dohnalová, K.; Pelant, I.; Valenta, J.; Fučíková, A.; Šídek, K.; Lang, J.; Englich, J.; Matějka, P.; Ztěpánek, P.; Bakardjieva, S. Brightly Luminescent Organically Capped Silicon Nanocrystals Fabricated at Room Temperature and Atmospheric Pressure. *ACS Nano* **2010**, *4*, 4494−4504.
(41) Chen, C.-C.; Dou, L.; Zhu, R.; Chung, C.-H.; Song, T.-B.; Zheng, Y. B.; Hawks, S.; Li, G.; Weiss, P. S.; Yang, Y. Visibly Transparent Polymer Solar Cells Produced by Solution Processing. *ACS Nano* **2012**, *6*, 7185−7190.

https://dx.doi.org/10.1021/acsami.0c12717
ACS Appl. Mater. Interfaces 2020, 12, 43771−43777